International Journal of Fatigue 72 (2015) 42–52

Contents lists available at ScienceDirect

International Journal of Fatigue

journal homepage: www.elsevier.com/locate/ijfatigue

Fatigue life of laser clad hardfacing alloys on AISI 4130 steel under rotary bending fatigue test

Novana Hutasoit [a,*], Vladimir Luzin [b], Aaron Blicblau [a], Wenyi Yan [c], Milan Brandt [d], Ryan Cottam [a]

[a] Industrial Research Institute Swinburne, Faculty of Engineering and Industrial Science, Swinburne University of Technology, Hawthorn, VIC 3122, Australia
[b] Australian Nuclear Science and Technology Organisation, Lucas Heights, New South Wales 2234, Australia
[c] Department of Mechanical and Aerospace Engineering, Monash University, Clayton, VIC 3800, Australia
[d] School of Aerospace, Mechanical and Manufacturing Engineering, RMIT University, Bundoora, VIC 3083, Australia

ARTICLE INFO

Article history:
Received 28 September 2013
Received in revised form 25 October 2014
Accepted 2 November 2014
Available online 13 November 2014

Keywords:
Laser cladding
Hardfacing coatings
Fatigue life
Neutron diffraction
Residual stresses

ABSTRACT

Fatigue life study of structures constructed by laser cladding using two types of hardfacing alloy, Stellite 6 (Co base) and Deloro 40G (Ni base) on AISI 4130 steel substrate was conducted using rotary bending fatigue test at ambient temperature 20 °C. The laser clad specimens showed a reduced fatigue life compared to the specimen without cladding but of the same size due to the presence of residual stresses in substrate and coating regions. The presence of higher compressive residual stresses in substrate region and lower tensile residual stress in coating region of specimen laser clad with Stellite 6 generated longer fatigue life compared to the specimens laser clad with Deloro 40G, at a similar coating thickness level. With the same final structure size, coating thickness produced an inversely proportional effect on fatigue life where thinner coatings result in less reduction of fatigue life compared to thicker coating. The analytical model employed in this study demonstrated that thinner coatings alters axial residual stress by generating lower tensile residual stress in coating region which enhance fatigue life, compared to thicker coatings. This work has demonstrated the influence of coating type, coating thickness and load level on the fatigue life of the laser clad structures.

1. Introduction

Laser cladding is a laser surfacing technique that can enhance the properties and/or regenerate the surface of a component. In laser cladding, laser radiation is absorbed and melts a small region of the substrate into which the coating material is injected and fuses the coating material to the substrate, thus producing a new layer (Fig. 1). Compared to other thermo-mechanical processes, laser cladding is identified to be superior in terms of its capability to produce lower dilution levels [1–3] and finer microstructure in clad layer [2,4], thus this technique has been implemented to enhance surface properties, i.e. increases surface hardness [5,6], wear resistance [3,7,8] and corrosion resistance [9,10]; refurbish deteriorated engineering component across different industries [4,11–16]; and perform rapid prototyping with the aid of numerically controlled equipment (CNC) [17]. Despite the extensive research on laser cladding for re-surfacing or rapid prototyping, little information can be found on fatigue life of structure constructed by laser cladding, a type of loading that many engineering components are exposed in service. Several studies have addressed fatigue life of structure constructed by laser cladding using uniaxial tensile-compression fatigue load [18] and bending fatigue load [19] which represent two of the types of loading applications for fatigue. However, the fatigue life behavior based on rotary bending loading, in particularly simulating a shaft refurbished by laser clad hardfacing alloys on its surface, has not been extensively investigated. The analysis of fatigue life is based on the alteration in residual stresses generated by laser cladding processes.

2. Experimental and numerical simulation

2.1. Laser cladding

The substrate and coating materials used in this experiment were AISI 4130 steel, Stellite 6 and Deloro 40G, respectively, with chemical composition shown in Table 1. Laser cladding was performed with a fiber delivered Nd:YAG Rofin Sinar laser, using a power of 550 W, a spot size 3 mm with a Gaussian beam profile and was shielded by Argon gas, with a scan speed of 500 mm/min. Stellite 6 and Deloro 40G powder was injected using an off-axis nozzle inclined at 60° to the substrate surface with powder

* Corresponding author. Tel.: +61 3 9214343; fax: +61 3 92145050.
E-mail address: nhutasoit@swin.edu.au (N. Hutasoit).

http://dx.doi.org/10.1016/j.ijfatigue.2014.11.001
0142-1123/

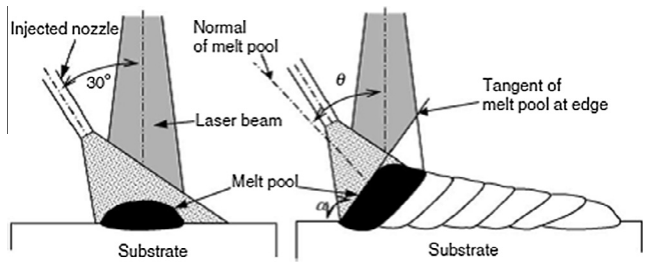

Fig. 1. Schematic illustration of single track and multi tracks laser cladding process [5].

feed rate of 4 g/min. Multiple tracks and multiple layers of Stellite 6 and Deloro 40G, each with powder size of 45–150 μm, were circumferentially deposited onto the surface of the grooved part of round bar AISI 4130 steel (Fig. 2).

2.2. Laser clad and fatigue test specimens manufacturing

The manufacturing of laser clad specimens were initiated by cutting a 12 mm diameter 4130 steel rod into 146 mm sections and followed by created groove at the middle of each section (Fig. 2). The diameter of grooved sections was set to three different size 5.5 mm, 6 mm and 6.5 mm that after laser cladding will create three different thickness of coating layer when cladding of the grooved section reaches the target diameter of minimum 8.3 mm. Smallest grooved section diameter (5.5 mm) is expected to generate the thickest coating layer (1.4 mm) while the largest grooved section diameter (6.5 mm) generate the thinnest coating layer (0.9 mm). Following the manufacturing of grooved section, multiple tracks with 70% overlap between track and multiple layers with 0.25 mm increment between each layer of Stellite 6 hardfacing alloy was laser clad onto the grooved section until the final grooved section diameter reached the minimum 8.3 mm, measured using Vernier caliper. Using the similar specimen geometry and laser processing parameters, sets of specimens were manufactured by deposited Deloro 40G hardfacing alloy on the grooved section of the specimens. This combination of initial groove diameters and laser cladding process parameters generated cladding layers with average thicknesses ranging from 1.06 to 1.82 mm in the machined fatigue samples.

Following the manufacturing of laser clad specimens, one specimen with grooved section diameter of 5.5 mm laser clad with Stellite 6 (specimen code STS) and one specimen laser clad with Deloro 40G (specimen code DS) were separated for residual stress measurement using neutron diffraction while others underwent a machining process to convert laser clad specimens to fatigue test specimens (Fig. 3). Along with laser clad specimens, substrate only (uncoated 4130 steel) also machined in order to manufacture fatigue test specimens (Fig. 3). All laser clad specimens that were machined down to fatigue test specimens geometry showed that coated region fully covered by coating material and no undercut was observed. This implied that the addition of 0.15 mm thick of coating layer that yielded 8.3 mm diameter on grooved section was sufficient to compensate dimensional distortion (e.g. bent) that occur during laser cladding process. Fatigue test specimens manufacturing was finalized by applying surface notch on the surface of substrate only (Fig. 4a) and on the surface coated specimen (Fig. 4b). The surface notch was made using wire cut method with a wire diameter of 0.25 mm, the depth of notch was 0.5 mm.

2.3. Metallography and hardness

The laser clad specimens were cut perpendicular to the laser clad track direction and ground-polished down to 1 μm. The samples were then etched in 2% Nital solution to reveal the microstructure of coating and heat affected zone at the vicinity of interface (location C and H in Fig. 4b). The Stellite 6 and Deloro 40G were electrolytically etched in 2% Nital solution using a circuit voltage of 8–10 mV. Micro-Vickers hardness measurements were performed using Buehler Micro Hardness Tester unit under 100 g load to measure the hardness of the coating and the substrate.

2.4. Residual stress measurement

Considering the fact that bending of a solid cylindrical object generates tension and compression along its axial direction, therefore the main interest of this research is to measure the axial residual stress that affecting the tension and compression stresses in axial direction of the specimen.

Table 1
Chemical composition of AISI 4130 steel, Stellite 6 and Deloro 40G.

	Composition (wt%)										
	Fe	C	Mn	P	S	Si	Cr	Mo	Co	Ni	W
AISI 4130 [47]	Bal	0.28–0.33	0.40–0.60	0.035 max	0.04 max	0.15–0.30	0.80–1.10	0.15–0.25			
Chemical composition Stellite 6											
Stellite 6 [48]	3	1.2	1			1.5	29	1.5	Bal	3	4.5
Deloro 40G[a]	1.5	0.35				3.5	7.5			Bal	1.7

[a] Material Safety Data Sheet (MSDS) of Deloro 40G.

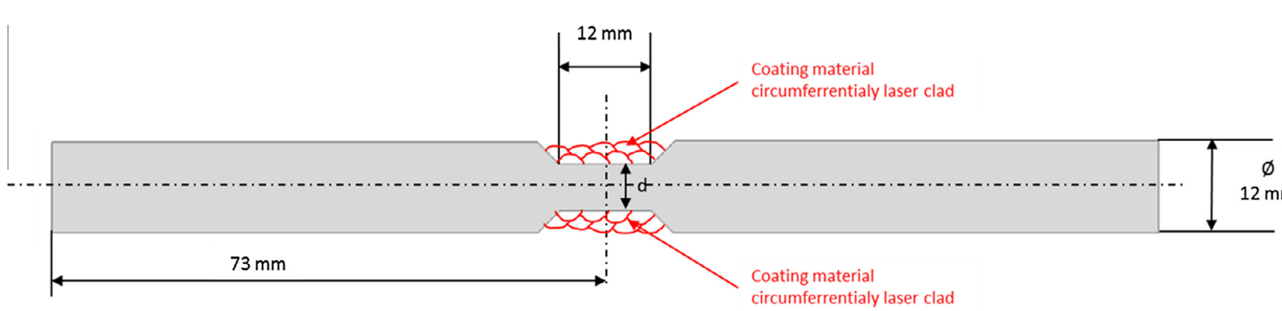

Fig. 2. Laser cladding specimen geometry. Diameter of grooved section (d) are 5.5 mm (S), 6 mm (M) and 6.5 mm (B).

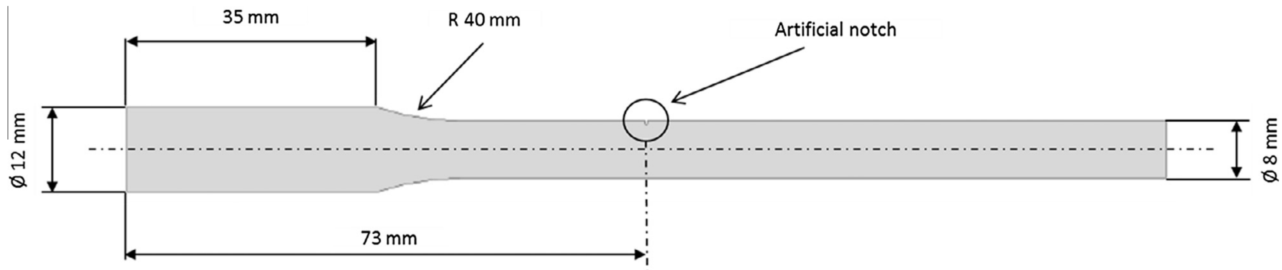

Fig. 3. Fatigue test specimen geometry for substrate only and laser clad. Artificial surface notch was applied on the surface of uncoated substrate AISI 4130 steel and on the surface of laser clad region of specimens laser clad with Stellite 6 and Deloro 40G.

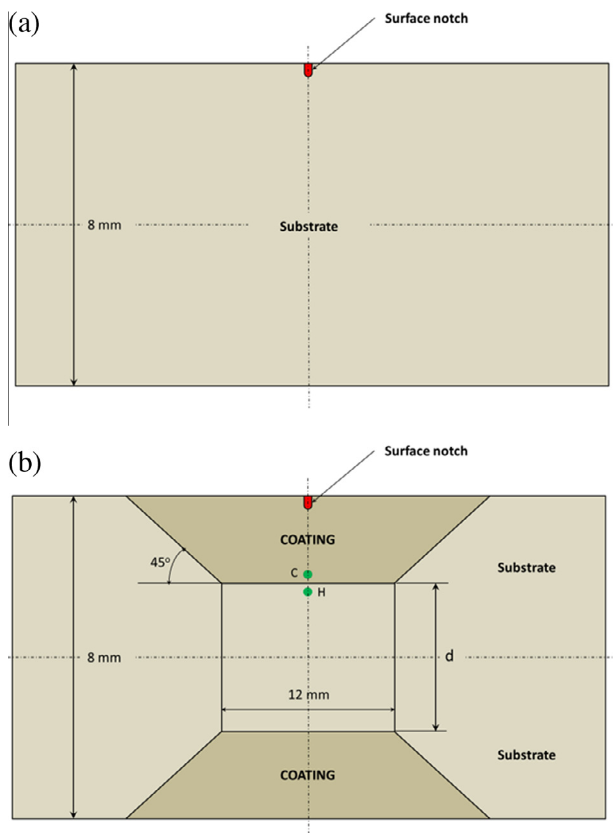

Fig. 4. Longitudinal cross section area at the vicinity of surface notch region in (a) substrate only specimen; (b) laser clad specimen, *d* indicate initial grooved section diameter (5.5 mm, 6 mm and 6.5 mm). Microstructure observation was performed at location C (in coating region) and H (in heat affected zone).

2.4.1. Residual stress measurement using neutron diffraction strain scanner

Strain scanning using neutron diffraction technique was performed on one specimen with grooved section diameter of 5.5 mm (coating thickness target 1.4 mm) laser clad with Stellite 6 (specimen code STS) and one specimen laser clad with Deloro 40G (specimen code DS). These two laser clad specimens were not undergone machining process. Due to the cylindrical geometry of the specimen used in this study, the residual stresses generated due to laser cladding were decomposed into radial stress (σ_R), hoop stress (σ_H) and axial stress (σ_A) (Fig. 5). Prior to residual stress calculation, strain scanning to measure the magnitude of strain generated inside the specimen was performed in three different direction, strain in radial (ε_R), hoop (ε_H) and axial (ε_A), according to these stress directions.

Upon specimen installation on the sample table, a series of intensity scan to measure the neutron counts by changing scan time with a given gauge volume, were performed to obtain statistically relevant neutron counts, where higher neutron counts yield a better accuracy and resolution. After a series of intensity scans, a program code was set up for strain scanner to automatically perform inter planar spacing (*d*-spacing) in substrate and coating region (Fig. 6). With reference to measured *d*-spacing obtained from strain scan, each component strain (ε_A, ε_R, ε_H) were calculated using equations

$$\varepsilon_A = \frac{(d_A - d_o)}{d_o}\ \text{(Axial)} \tag{1}$$

$$\varepsilon_R = \frac{(d_R - d_o)}{d_o}\ \text{(Radial)} \tag{2}$$

$$\varepsilon_H = \frac{(d_H - d_o)}{d_o}\ \text{(Hoop)} \tag{3}$$

Then using of Poisson's ratio and elastic modulus with strain information, the stress in the three directions was calculated using the following equations [20]

$$\sigma_R = \frac{E}{(1+\nu)(1-2\nu)}\{\varepsilon_R(1-\nu)+\nu(\varepsilon_H+\varepsilon_A)\}\ \text{(Radial direction)} \tag{4}$$

$$\sigma_H = \frac{E}{(1+\nu)(1-2\nu)}\{\varepsilon_H(1-\nu)+\nu(\varepsilon_A+\varepsilon_R)\}\ \text{(Hoop direction)} \tag{5}$$

$$\sigma_A = \frac{E}{(1+\nu)(1-2\nu)}\{\varepsilon_A(1-\nu)+\nu(\varepsilon_R+\varepsilon_H)\}\ \text{(Axial direction)} \tag{6}$$

Since a high neutron count was only observed in the 4130 steel substrate region during intensity scan stage, accuracy of residual measurement is only available for this region. The parameters of d_o, E and ν of 1.731 Å, 224 GPa and 0.289 respectively, calculated from the data obtained in strain scanning stage were used to estimate the magnitude of the residual stresses in substrate region. As for the residual stresses measurement in Stellite 6 coating, the parameter of d_o, E and ν of 1.089 Å, 214.38 GPa and 0.302 respectively, were employed. In order to measure the residual stress in Deloro 40G coating, the parameter of d_o, E and ν of 1.075 Å, 214.38 GPa and 0.302 respectively, were employed. Following the measurement of residual stress using neutron diffraction technique, an analytical model was also employed to estimate the magnitude of the residual stresses, elucidated in Section 2.4.2.

Residual stress measurements using neutron diffraction technique in this research was performed on KOWARI neutron diffraction strain scanner at Australian Nuclear Science and Technology Organization (ANSTO), Lucas Heights, New South Wales, Australia.

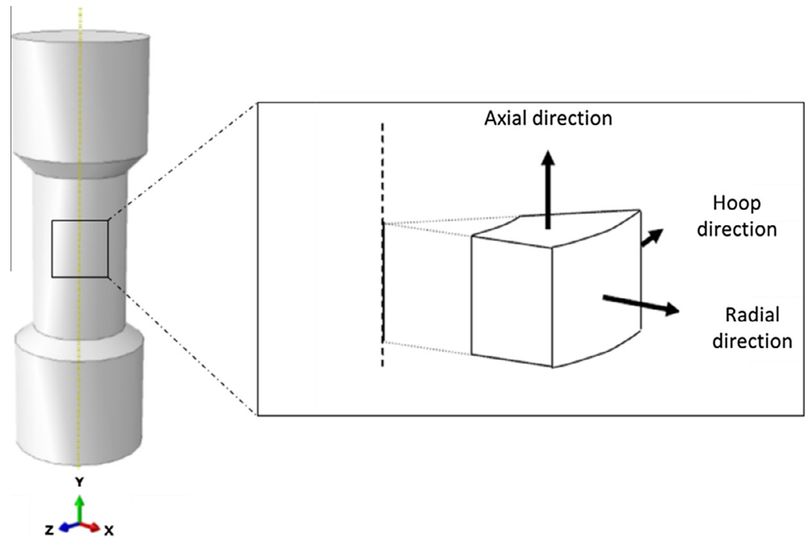

Fig. 5. Stresses in solid cylindrical object.

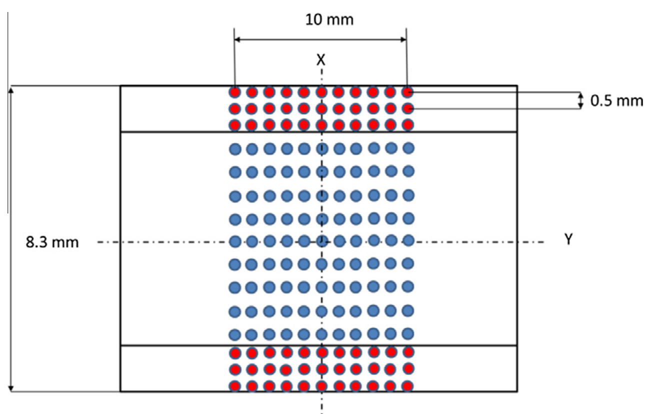

Fig. 6. Schematic layout of strain scan location in specimen, refer to longitudinal (*y*-axis) cross section cut at the center of laser clad specimen (Fig. 2). Red dots represent strain scan location in coating region while blue dots represent strain scan in substrate region. (For interpretation of the references to color in this figure legend, the reader is referred to the web version of this article.)

2.4.2. Residual stress numerical modeling

Numerical modeling of residual stress formation in laser clad specimens was performed using a model developed by Tsui and Clyne [21] which analytically models residual stress formation in coated cylindrical geometry specimens. This analytical model not only took into account the dimension of coating and the substrate, but also the deposition stress of coating material; and coefficient of thermal expansion (CTE) of the coating and the substrate in calculating the magnitude and sign of the residual stresses. The deposition stress is defined as the unbalanced stress in the layer before it comes into equilibrium with the underlying material, at a particular substrate temperature [21], in which this unbalance stress causes misfit strains that for a coated specimen, is expressed as

$$\Delta\varepsilon = \frac{\sigma_d}{E_d} \tag{7}$$

where $\Delta\varepsilon$ is the misfit strain, σ_d is the deposition stress and E_d is the elastic modulus of the coating. The definition of deposition stress also implies that the deposition of consecutive layer(s) affects the misfit strain and in turn affects the stress generated in the substrate and in the subsequent layer in the three directions, axial, radial and hoop. The elastic modulus of Stellite 6 and Deloro 40G employed in this study are considered as isotropic with value of 213 GPa [22] and 206.9 GPa [22], respectively. The other factor accounts for the formation of residual stress is the thermal contraction effect that causes misfit strain between deposited layers with the underlying material. In the case of coated substrate, misfit strain due to thermal contraction effect is expressed as [21]

$$\Delta\varepsilon = (\alpha_s - \alpha_d)\Delta T \tag{8}$$

where α_s is the substrate's CTE, α_d is the coating's CTE, ΔT is the temperature difference between initial temperature and final temperature. The initial temperature can be the deposition temperature while the final temperature is the temperature when the specimen has undergone cooling process down to ambient temperature. As in residual stress formation due to deposition stress, the deposition of consecutive layer(s) affects the residual stress formation in substrate and in subsequent layer(s) that in turn affects the total residual stresses formed in the coated specimen. Coefficient of thermal expansion of different material employed in this study is presented in Table 2.

Table 2
Coefficient of thermal expansion (CTE) of selected materials.

Material	Coefficient of thermal expansion (CTE) (μ/°K)	Temperature range (°C)
AISI 4130 [49]	12.2 (at 20 °C), 14.2 (at 600 °C)	20–600
Stellite 6 [50]	11.35, 12.95, 13.6, 13.9, 14.2, 14.5, 14.7, 15.05, 15.5, 17.5	100–1000
Deloro 40G[a] [51]	11.14, 12.49, 13.05, 13.56, 14.15, 14.70, 15.24, 16.22	100–800

[a] Based on Inconel 617 material.

The detail derived equations, constants and assumptions of the residual stress analytical model are presented in [21]. Considering the concepts employed in the model developed by Tsui and Clyne [21], this analytical model is capable to predict the magnitude and the sign of the residual stresses in coating region, after laser cladding process and furthermore capable to predict the change of the magnitude of residual stresses when incorporating changes in the dimension of substrate and coating.

2.5. Fatigue test

Fatigue tests were performed on cantilever type rotary bending test rig (Fig. 7), under load of 100 N, 150 N and 200 N, with loading

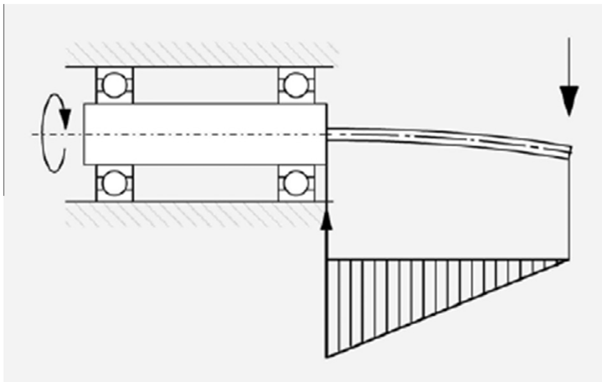

Fig. 7. Schematic of cantilever type rotary bending fatigue test rig.

ratio (R) of -1. Fatigue test rig was driven by electric motor operating in 2850 rpm.

In this study, the presence of artificial notch on the surface of uncoated substrate and on the laser clad region of fatigue test specimen (Fig. 3) provide the crack initiation site for further crack propagation during fatigue loading, therefore fatigue life investigation was based on crack propagation stage until the specimens fractured. Uncoated substrate AISI 4130 steel specimens were employed as the reference in studying the effect of different type of coating materials and thicknesses on fatigue life of laser clad specimens. The actual coating thickness was measured on the surface of fractured specimen after fatigue test (Fig. 8).

Fatigue life analysis was performed using Weibull distribution analysis due to its ability to be used with small sample sizes when fitting the data [23]. Prior to implementing the Weibull distribution in fatigue life analysis, the relationship between load amplitude and fatigue life of, is presented as an S–N diagram which is implemented in rotary bending fatigue test of uniform material and surface treated material [24–29], which can be presented in an equation that follow power law function

$$\sigma_a = a(N_f)^b \tag{9}$$

where σ_a is the load amplitude, N_f is fatigue life and a, b are the power equation constants. Due to small number of specimens tested (3 specimens per condition), fatigue life is analyzed by calculating the mean fatigue life of each condition using maximum likelihood estimation (MLE) approach.

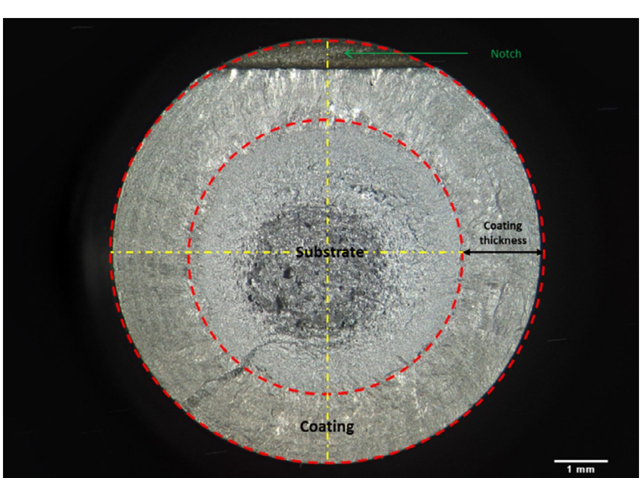

Fig. 8. Fracture surface of laser clad specimen.

3. Results and discussion

3.1. Microstructure and micro Vickers hardness

The microstructure of Stellite 6 coating obtained in this experiment is a mixture of dendrites (bright color) structure that is rich with Co [30–32] and inter-dendritic structure (dark color) (Fig. 9) rich with eutectic carbide [31–35] formed by a eutectic reaction. Microstructure of heat affected zone (HAZ) for the specimen coated with Stellite 6, shown in Fig. 10, consists of ferrite (white color phase), pearlite (dark color phase) and tempered martensite or bainite (gray color phase). The microstructure in the coating area and the heat affected zone of the specimen coated with Deloro 40G is shown in Figs. 11 and 12 respectively. The microstructure of Deloro 40G coating obtained in this experiment is a mixture of dendritic (bright color) structure rich in Ni [36] and inter-dendritic structure (dark color) (Fig. 10) rich with carbide [36,37].

Form Fig. 13, it can be observed that coating region is harder than substrate region. This higher hardness level is contributed by the presence of carbides in dendritic and inter dendritic structure (Figs. 8 and 10) as the result of higher content of strong carbide forming elements (Co, Cr, W) in Stellite 6 and mainly Cr element in Deloro 40G compared to the ones in AISI 4130 (Table 1). As for coating region, Stellite 6 coating shows a higher hardness level than Deloro 40G coating due to the presence of a larger amount of hard carbides as result of more carbide forming elements (Table 1).

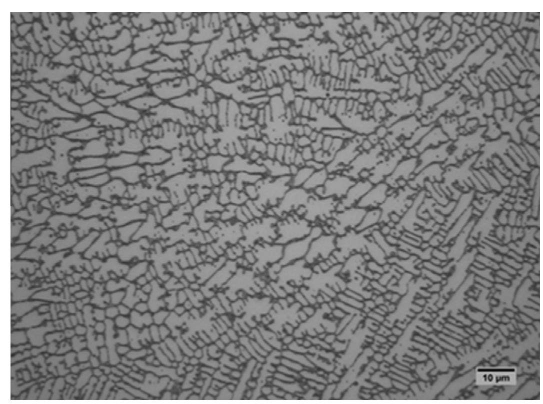

Fig. 9. Microstructure of coating at the vicinity of interface in specimen laser clad with Stellite 6 (specimen code STS).

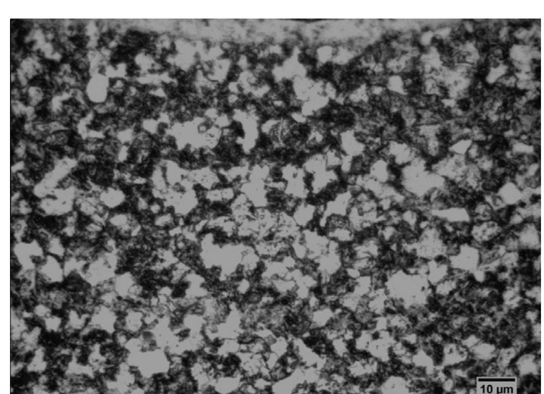

Fig. 10. Microstructure of HAZ in specimen laser clad with Stellite 6 (specimen code STS).

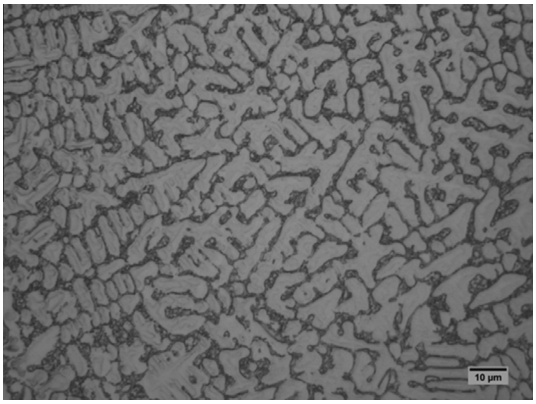

Fig. 11. Microstructure of coating at the vicinity of interface in specimen laser clad with Deloro 40G (specimen code DS).

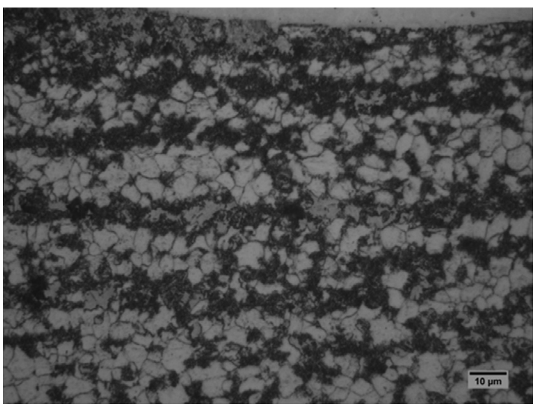

Fig. 12. Microstructure of HAZ in specimen laser clad with Deloro 40G (specimen code DS).

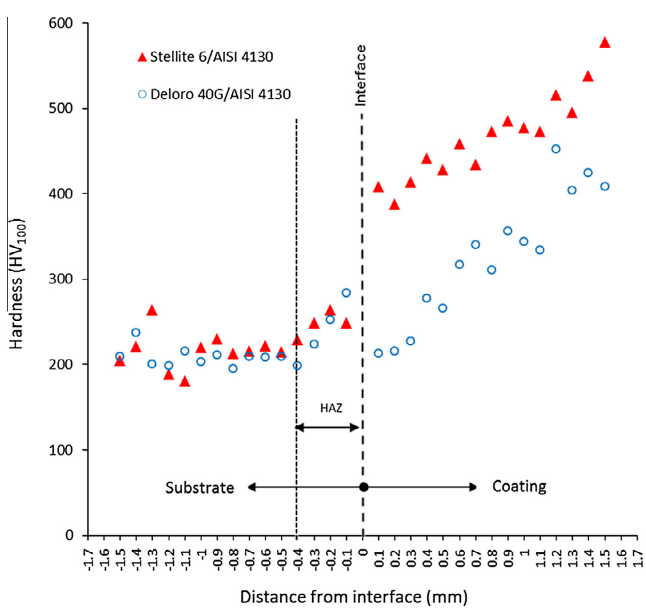

Fig. 13. Hardness profile of Stellite 6/AISI 4130 structure (specimen code STS) and Deloro 40G/AISI 4130 structure (specimen code DS).

3.2. Residual stress measured by neutron diffraction method

Due to its symmetrical geometry in the form of solid cylinder, residual stress data obtained in the measurement were presented in half geometry at different radial distances from center of specimen toward outer surface of specimen, as shown in Fig. 14. Residual stresses in substrate region of the specimen's laser clad with thick Stellite 6 and Deloro 40G were found in compressive type, in axial direction. In addition, higher compressive residual stresses were formed in substrate region in specimen coated with Stellite 6 compared to the specimens coated with Deloro 40G (Fig. 14). Contrary to a small fluctuation of axial residual stress in substrate region, coating region exhibited a large deviation of residual stress that distributed from +610 MPa to −538 MPa in Stellite 6 coating and from +359 MPa to −539 MPa in Deloro 40G coating (Fig. 14). In addition to the effect of the multiple layers of coating material laser clad onto steel substrate, it was also expected that the presence of Cobalt element in Stellite 6 and Boron element in Deloro 40G (Table 1), influenced the large deviation of residual stress measured in coating region. As indicated by low neutron count during intensity scan in coating region, Cobalt and Boron tend to absorb rather than diffracting the incoming neutron which is required in order to obtain more accurately measurement. Therefore, the measurement of strain changes in coating region was expected to yield a less accurate result.

3.3. Residual stresses from numerical modeling

3.3.1. Numerical modeling validation

Numerical modeling was performed by adjusting deposition stress value for each type of coating material in conjunction with coefficient of thermal expansion value of substrate and coating material (Table 2) until the calculated residual stress in axial direction is coincident with average value measured by using neutron diffraction. In addition, by taking into account the deviation of residual stresses measured by neutron diffraction at radial distance 0 mm, 0.5 mm and 1.0 mm in substrate region (Fig. 14), the profile of residual stress was found to be closer to a linear line that is used as the reference in validating the numerical modeling. The locations indicated by radial distance of 1.5 mm and 2.0 mm (Fig. 14) are located closer to interface between substrate and coating region where dilution takes place [38], which causes larger deviation of residual stresses compared to the regions closer to

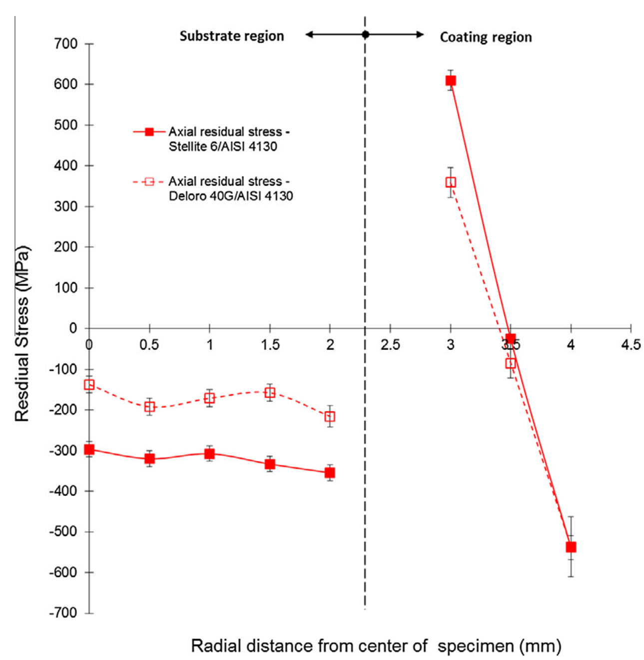

Fig. 14. Axial residual stresses in substrate and coating region of specimen coated with Stellite 6 (specimen code STS) and Deloro 40G (specimen code DS).

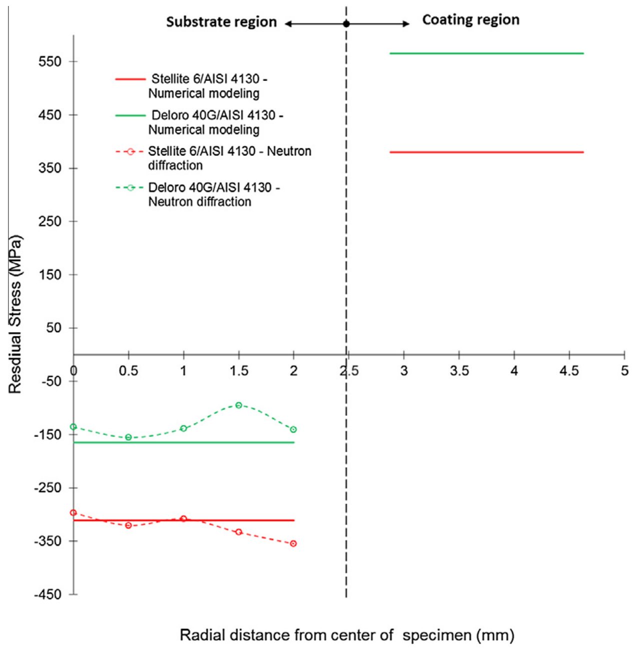

Fig. 15. Axial residual stresses in specimen laser clad with Stellite 6 and Deloro 40G, based on 1.5 mm coating thickness.

the center of the substrate. Therefore measured residual stresses at locations close to interface were not referred to validate numerical modeling approach.

Numerical modeling of axial residual stress in substrate region that was calibrated by the result obtained by neutron diffraction method is contained in Fig. 15. From this figure, it can be observed that calculated axial residual stress in substrate region of specimen laser clad with Stellite 6 is in good agreement with the result obtained through neutron diffraction method. In the case of specimen laser clad with Deloro 40G, calculated axial residual in substrate region was found approximately 7% differ from the result obtained through neutron diffraction. This implied that after calibration, the analytical model employed in this study is found adequate to estimate the magnitude of residual stress in the substrate region and provided a reasonable estimation of the magnitude of residual stress in coating region. Analytical model employed in this study estimated the magnitude of axial residual stress generated in Stellite 6 coating region was +380 MPa (Fig. 15), lies in the upper portion of residual stress range measured by neutron diffraction method (Fig. 14). For comparison purpose, this magnitude of axial residual stress was found lower than tensile residual stress in Stellite 6 laser clad on tool steel, around +450 MPa that was measured using X-ray diffraction method [39]. This discrepancy is expected to contribute by different type of steel substrate used in the experiment that lead to different CTE; and different geometry of laser clad specimen employed in each study where these two factors influence the formation of residual stress. In addition, since X-ray diffraction method tends to estimate the residual stress higher than estimated by neutron diffraction method [40–42], the numerical modeling employed in this study that was calibrated by neutron diffraction result, provided a reasonable estimate of the magnitude of residual stress in coating region. As for the other type of coating material, the analytical model employed in this study estimated the magnitude of axial residual stress generated in Deloro 40G coating was +565 MPa (Fig. 15), higher than the maximum axial tensile residual stress measured by neutron diffraction method (Fig. 14).

3.3.2. Effect of coating material

From Fig. 15, it can be observed that specimens laser clad with Stellite 6 tend to generate higher compressive residual stress in substrate region and lower tensile residual stresses in coating region, in axial direction when compared to specimen laser clad with Deloro 40G. This can be contributed to the difference of coefficient of thermal expansion (CTE) at high temperature of Stellite 6 and Deloro 40G compared to AISI 4130 substrate (Table 2). The difference in CTE between AISI 4130 and Stellite 6 is lower than between AISI 4130 and Deloro 40G, thus a lower strain misfit between occurs between the two material (Eq. (8)) that leads to a lower level of residual stresses formed (Fig. 15). Whereas for the Deloro 40G there is a larger difference in CTE between AISI 4130 and Deloro 40G structure which forms a larger strain misfit that leads to higher residual stresses generated in the structure.

3.3.3. Effect of coating thickness

In this study, coating thickness was varied by a combination of the specimen's initial diameter and number of coating layers applied so that the outer diameter of the clad specimens was consistent. Specimen's initial diameter is the diameter of region in the specimen that is laser clad with coating materials (Fig. 2), in this experiment, three groups of specimens prepared where different initial diameters were assigned, 5.5 mm, 6.0 mm and 6.5 mm. Number of coating layers applied is the total number of coating layer applied in the manufacturing of laser clad specimen before being machined down to manufacture the fatigue test specimens. Therefore, in order to manufacture the laser clad specimen, 8 layers of coating laser clad on specimen with small diameter (5.5 mm) and a less number of coating layers on specimen with a larger diameter (6.5 mm).

Parametric study on residual stress formation in laser clad specimen revealed that the magnitude of axial residual stress in sub-

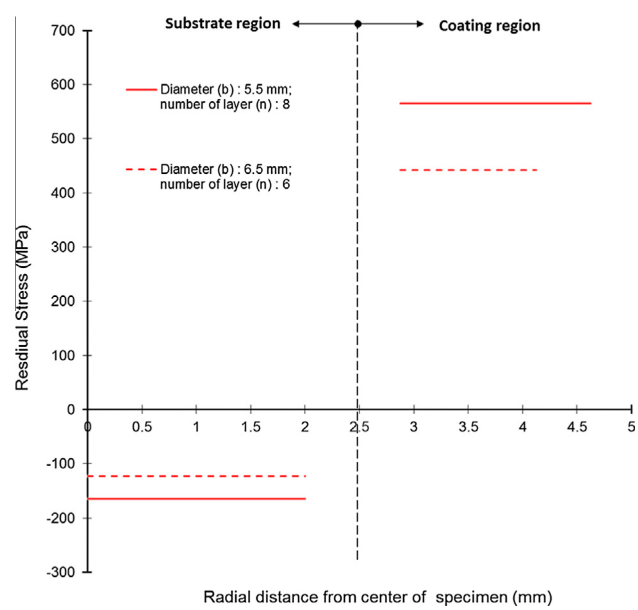

Fig. 16. Effect of initial radii (b) and number of layers (n) on axial residual stress formation based on laser clad Deloro40G on AISI 4130 structure.

Table 3
Thickness of coating.

Specimen code	Average thickness[a] (mm)
STS	1.46
STM	1.29
STB	1.06
DS	1.82
DM	1.58
DB	1.30

[a] Coating thickness was measured on actual specimen's fracture surface.

Table 4
Fatigue life calculation for uncoated substrate AISI 4130 steel specimens and specimens laser clad with Stellite 6 and Deloro 40G, using Weibull method.

Coating material/thickness (mm)	Load (N)	Fatigue life			Scale parameter (η)			Shape parameter (β)		
		Data	Mean	Standard deviation	Expected	Lower 95% confidence limit	Upper 95% confidence limit	Expected	Lower 95% confidence limit	Upper 95% confidence limit
Uncoated substrate AISI 4130 steel	200	55,729 53,523 51,336	53,520	1970	54,400	52,820	56,020	34.14	16.01	72.82
	150	105,901 120,444 120,588	116,100	5863	118,700	114,000	123,500	24.69	10.38	58.73
	100	500,645 424,412 412,589	445,000	45,770	464,700	426,500	506,200	11.8	5.686	24.48
Stellite 6/1.46	200	25,474 18,465 18,711	20,850	3641	22,340	19,220	25,960	6.715	3.241	13.91
	150	53,411 44,455 47,752	48,490	4166	50,300	46,870	53,990	14.25	6.776	29.95
	100	209,507 194,138 232,726	212,000	17,690	219,700	205,100	235,200	14.69	6.964	30.97
Stellite 6/1.29	200	39,789 40,250 41,750	40,570	1028	41,030	40,200	41,860	49.9	23.98	103.9
	150	113,007 106,747 109,368	109,100	2822	110,400	108,600	112,200	48.89	27.52	86.84
	100	250,102 215,106 220,441	228,100	18,340	236,100	221,000	252,300	15.27	7.358	31.7
Stellite 6/1.06	200	82,696 78,440 64,775	75,600	6975	78,620	72,920	84,760	13.23	5.806	30.13
	150	143,888 157,426 124,508	142,100	13,610	148,000	136,800	160,100	12.72	5.843	27.68
	100	186,769 386,375 268,923	279,400	83,970	309,600	236,100	406,000	3.707	1.733	7.928
Deloro 40G/1.82	200	3,776 2894 3121	3259	422	3437	3082	3833	9.25	4.434	19.29
	150	4927 5319 7725	5834	1128	6288	5317	7437	6.017	2.896	12.5
	100	58,847 53,459 41,764	51,560	6724	54,390	48,790	60,640	9.179	4.107	20.52
Deloro 40G/1.58	200	8724 8171 8590	8504	219	8602	8429	8779	48.94	21.61	110.8
	150	18,871 19,163	17,910	1458	18,550	17,370	19,810	15.07	6.37	35.66

(*continued on next page*)

Table 4 (*continued*)

Coating material/thickness (mm)	Load (N)	Fatigue life			Scale parameter (η)			Shape parameter (β)		
		Data	Mean	Standard deviation	Expected	Lower 95% confidence limit	Upper 95% confidence limit	Expected	Lower 95% confidence limit	Upper 95% confidence limit
	100	15,420 105,583 106,024 150,834	120,700	23,490	130,100	109,800	154,100	5.969	2.881	12.36
Deloro 40G/1.30	200	9607 11,629 19,335	13,560	4295	15,070	11,290	20,110	3.497	1.677	7.29
	150	62,871 56,361 39,417	53,180	9091	56,910	49,230	65,780	6.871	3.033	15.57
	100	200,071 217,665 178,966	199,000	16,440	206,200	192,700	220,600	14.84	6.887	31.99

strate and coating region was altered by coating thickness while maintaining constant deposition stress and coefficient of thermal expansion of substrate and coating material. Thick coating was produced by applying 8 layers of coating on the surface of grooved section with diameter of 5.5 mm while thin coating was produced by applying 6 layers of coating on the surface of grooved section with diameter of 6.5 mm.

In the case of thinly coated specimens constructed by using a larger initial diameter specimen and applying a less number of coating layers, it was estimated that lower compressive residual stresses in substrate region and lower tensile residual stress in coating region, in axial stress direction, were generated (Fig. 16). In contrary to thin coated specimen, the thick coated specimen constructed by using small initial diameter and applying more coating layers, exhibited the opposite trend (Fig. 16).

3.4. Fatigue life

Coating thickness data is contained in Table 3 while fatigue life calculation based on Weibull method of uncoated substrate AISI 4130 steel specimens and specimens laser clad with Stellite 6 and Deloro 40G is contained in Table 4; and presented in the form of S–N curve in Fig. 17.

3.4.1. Effect of type of coating material on fatigue life

Fatigue life comparative study between specimen laser clad with Stellite 6 and Deloro 40G shows that for similar coating thicknesses, specimen laser clad with Stellite 6 exhibited a longer fatigue life compared to the specimen laser clad with Deloro 40G (Fig. 17). This can be contributed to the difference of coefficient of thermal expansion (CTE) at high temperature of Stellite 6 and Deloro 40G compared to AISI 4130 substrate (Table 2) that yield different level of residual stress generated in substrate and coating region. Numerical simulation of residual stresses formation as the result of different CTE (Table 2) has revealed that specimens laser clad with Stellite 6 generated higher compressive residual stresses in substrate region and lower tensile residual stresses in coating region, in axial stress direction, compared to the specimen laser clad with Deloro 40G (Fig. 15). The presence of tensile residual stress is detrimental to fatigue life while compressive residual stress enhances fatigue life [43–46].

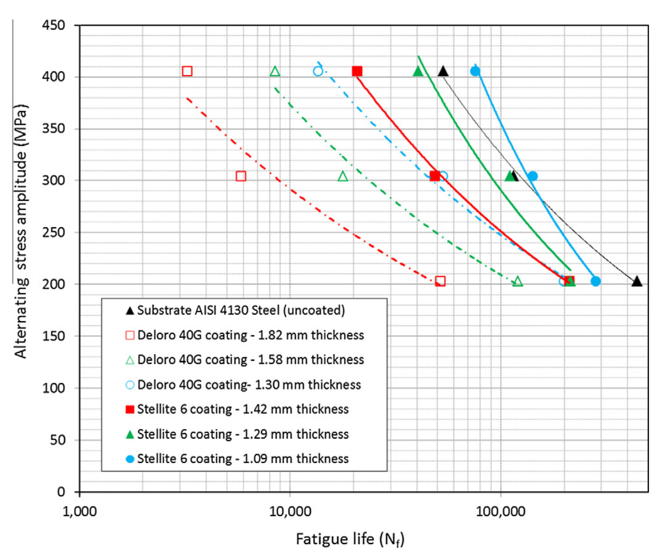

Fig. 17. S–N curves for uncoated substrate AISI 4130 steel specimens and specimens laser clad with Stellite 6 and Deloro 40G coating material.

3.4.2. Effect of coating thickness on fatigue life

From the fatigue tests, it is evident that fatigue life of specimen laser clad with Stellite 6 and Deloro 40G is inversely proportional to coating thickness where fatigue life decreases when the coating thickness increases (Fig. 17). This phenomenon is expected to be contributed by the change in residual stress in the substrate and coating region after laser cladding. As estimated by the analytical model employed in this study, thin coated specimen showed larger reduction of tensile residual stress in coating region than the reduction of compressive residual stress in substrate region, in axial stress direction (Fig. 16). Therefore, the presence of compressive residual stress in substrate region in conjunction with lower tensile residual stress in coating region, in axial stress direction, enhanced the fatigue life of thin coated specimens.

4. Conclusion

Fatigue behavior of laser clad hardfacing alloys on AISI 4130 steel has been examined, and the following conclusions can be drawn from this study:

1. Specimen constructed by laser clad Stellite 6 (Co base) and Deloro 40G (Ni base) on AISI 4130 steel to a certain size showed decrease in fatigue life compared to specimen of the same size without cladding, due to the presence of tensile residual stress in coating area of laser clad specimen.
2. The presence of higher compressive residual stress in substrate region and lower tensile residual stresses in coating region in specimen laser clad with Stellite 6 generated longer fatigue life compared to the specimens laser clad with Deloro 40G, at similar coating thickness levels.
3. With the same final structure size, increasing the coating thickness reduced the fatigue life of laser clad specimens as the result of tendency toward the presence of higher tensile residual stress in axial stress direction in coating region.

Acknowledgements

The author gratefully acknowledges Mr. Brian Dempster and Mr. Girish Thirreduperapa from Swinburne University of Technology for conducting the laser cladding process using the ND:YAG laser; and Australian Institute of Nuclear Science and Engineering (AINSE) for funding the neutron diffraction beam time under proposal number P2502.

References

[1] Xu G, Kutsuna M, Liu Z, Yamada K. Comparison between diode laser and TIG cladding of Co-based alloys on the SUS403 stainless steel. Surf Coat Technol 2006;201:1138–44.
[2] Kathuria YP. Some aspects of laser surface cladding in the turbine industry. Surf Coat Technol 2000;132:262–9.
[3] Atamert S, Bhadeshia H. Comparison of the microstructures and abrasive wear properties of stellite hardfacing alloys deposited by arc welding and laser cladding. Metall Mater Trans A 1989;20:1037–54.
[4] Shepeleva L, Medres B, Kaplan WD, Bamberger M, Weisheit A. Laser cladding of turbine blades. Surf Coat Technol 2000;125:45–8.
[5] Sun S, Durandet Y, Brandt M. Parametric investigation of pulsed Nd: YAG laser cladding of stellite 6 on stainless steel. Surf Coat Technol 2005;194:225–31.
[6] Barnes S, Timms N, Bryden B, Pashby I. High power diode laser cladding. J Mater Process Technol 2003;138:411–6.
[7] So H, Chen CT, Chen YA. Wear behaviours of laser-clad stellite alloy 6. Wear 1996;192:78–84.
[8] Sha C-K, Tsai H-L. Hardfacing characteristics of S42000 stainless steel powder with added silicon nitride using a CO_2 laser. Mater Charact 2004;52:341–8.
[9] Chen C, Zhang M, Chang Q-M, Zhang S, Ma H-Y, Yan W-Q, et al. Laser cladding of ZM5 magnesium base alloy with Al+Nano-SiC powder. In: Lasers in engineering (Old City Publishing), Old City Publishing Inc; 2008. p. 85–94.
[10] Volovitch P, Masse JE, Fabre A, Barrallier L, Saikaly W. Microstructure and corrosion resistance of magnesium alloy ZE41 with laser surface cladding by Al–Si powder. Surf Coat Technol 2008:4901–14.
[11] Bendeich P, Alam N, Brandt M, Carr D, Short K, Blevins R, et al. Residual stress measurements in laser clad repaired low pressure turbine blades for the power industry. Mater Sci Eng A 2006:70–4.
[12] Sexton L, Lavin S, Byrne G, Kennedy A. Laser cladding of aerospace materials. J Mater Process Technol 2002;122:63–8.
[13] Xiong Z, Chen G-X, Zeng X-Y. Effects of process variables on interfacial quality of laser cladding on aeroengine blade material GH4133. J Mater Process Technol 2009;209:930–6.
[14] Richter K, Orban S, Nowotny S. Laser cladding of the titanium alloy Ti6242 to restore damaged blades. In: 23rd International congress on applications of lasers and electro-optics, San Francisco; 2004.
[15] Niederhauser S, Karlsson B. Fatigue behaviour of Co–Cr laser cladded steel plates for railway applications. Wear 2005:1156–64.
[16] Sun Y, Hanaki S, Yamashita M, Uchida H, Tsujii H. Fatigue behavior and fractography of laser-processed hot work tool steel. Vacuum 2004:655.
[17] Nath AK. Indigeneously developed CO_2 lasers in material processing applications. CURIE 2008;1:26–32.
[18] Niederhauser S, Karlsson B. Fatigue behaviour of Co–Cr laser cladded steel plates for railway applications. Wear 2005;258:1156–64.
[19] Koehler H, Partes K, Seefeld T, Vollertsen F. Influence of laser reconditioning on fatigue properties of crankshafts. Phys Procedia 2011;12(Part A):512–8.
[20] Ju DY, Mukai R, Minakawa N, Morii Y, Moriai A. A measurement method of residual stress in quenched steel by neutron diffraction. Key Eng Mater 2004:139–45.
[21] Tsui YC, Clyne TW. An analytical model for predicting residual stresses in progressively deposited coatings Part 2: cylindrical geometry. Thin Solid Films 1997;306:34–51.
[22] Cockeram B. The fracture toughness and toughening mechanisms of nickel-base wear materials. Metall Mater Trans A 2002;33:33–56.
[23] Dodson B. The Weibull analysis handbook. 2nd ed. Milwaukee: American Society for Quality; 2006.
[24] Papakyriacou M, Mayer H, Pypen C, Plenk H, Stanzl-Tschegg S. Influence of loading frequency on high cycle fatigue properties of b.c.c. and h.c.p. metals. Mater Sci Eng, A 2001;308:143–52.
[25] Nascimento MP, Souza RC, Pigatin WL, Voorwald HJC. Effects of surface treatments on the fatigue strength of AISI 4340 aeronautical steel. Int J Fatigue 2001;23:607–18.
[26] Farfán S, Rubio-González C, Cervantes-Hernández T, Mesmacque G. High cycle fatigue, low cycle fatigue and failure modes of a carburized steel. Int J Fatigue 2004;26:673–8.
[27] Genel K, Demirkol M, Çapa M. Effect of ion nitriding on fatigue behaviour of AISI 4140 steel. Mater Sci Eng, A 2000;279:207–16.
[28] Sohar CR, Betzwar-Kotas A, Gierl C, Weiss B, Danninger H. Gigacycle fatigue behavior of a high chromium alloyed cold work tool steel. Int J Fatigue 2008;30:1137–49.
[29] Sun Y, Hanaki S, Yamashita M, Uchida H, Tsujii H. Fatigue behavior and fractography of laser-processed hot work tool steel. Vacuum 2004;73:655–60.
[30] Xu GJ, Kutsuna M. Characteristics of multilayer laser cladding using powder mixture of Co based alloy and vanadium carbide. Mater Sci Technol 2008;24:73–84.
[31] Lin WC, Chen C. Characteristics of thin surface layers of cobalt-based alloys deposited by laser cladding. Surf Coat Technol 2006;200:4557–63.
[32] Xu GJ, Kutsuna M. Cladding with Stellite 6 + WC using a YAG laser robot system. Surf Eng 2006;22:345–52.
[33] de Oliveira U, Ocelík V, De Hosson JTM. Residual stress analysis in Co-based laser clad layers by laboratory X-rays and synchrotron diffraction techniques. Surf Coat Technol 2006;201:533–42.
[34] d'Oliveira ASCM, Vilar R, Feder CG. High temperature behaviour of plasma transferred arc and laser Co-based alloy coatings. Appl Surf Sci 2002;201:154–60.
[35] Shin J-C, Doh J-M, Yoon J-K, Lee D-Y, Kim J-S. Effect of molybdenum on the microstructure and wear resistance of cobalt-base Stellite hardfacing alloys. Surf Coat Technol 2003;166:117–26.
[36] Ming Q, Lim LC, Chen ZD. Laser cladding of nickel-based hardfacing alloys. Surf Coat Technol 1998;106:174–82.
[37] Liu X-B, Fu G-Y, Liu S, Shi S-H, He X-M, Wang M-D. High temperature wear and corrosion resistance of Co-free Ni-based alloy coatings on nuclear valve sealing surfaces. Nucl Eng Des 2011;241:4924–8.
[38] Hutasoit N, Yan W, Cottam R, Brandt M, Blicblau A. Evaluation of microstructure and mechanical properties at the interface region of laser-clad stellite 6 on steel using nanoindentation. Metallogr Microstruct Anal 2013;2:328–36.
[39] Grum J, Žnidaršič M. Microstructure, microhardness, and residual stress analysis of laser surface cladding of low-carbon steel. Mater Manuf Process 2004;19:243–58.
[40] Ganguly S, Stelmukh V, Edwards L, Fitzpatrick ME. Analysis of residual stress in metal-inert-gas-welded Al-2024 using neutron and synchrotron X-ray diffraction. Mater Sci Eng, A 2008;491:248–57.
[41] Martinez-Perez ML, Mompean FJ, Ruiz-Hervias J, Borlado CR, Atienza JM, Garcia-Hernandez M, et al. Residual stress profiling in the ferrite and cementite phases of cold-drawn steel rods by synchrotron X-ray and neutron diffraction. Acta Mater 2004;52:5303–13.

[42] Menig R, Pintschovius L, Schulze V, Vöhringer O. Depth profiles of macro residual stresses in thin shot peened steel plates determined by X-ray and neutron diffraction. Scripta Mater 2001;45:977–83.
[43] Withers PJ. Residual stress and its role in failure. Rep Prog Phys 2007;70:2211.
[44] Jendrzejewski R, Śliwiński G, Krawczuk M, Ostachowicz W. Temperature and stress during laser cladding of double-layer coatings. Surf Coat Technol 2006;201:3328–34.
[45] Montross CS, Wei T, Ye L, Clark G, Mai Y-W. Laser shock processing and its effects on microstructure and properties of metal alloys: a review. Int J Fatigue 2002;24:1021–36.
[46] Ruschau JJ, John R, Thompson SR, Nicholas T. Fatigue crack nucleation and growth rate behavior of laser shock peened titanium. Int J Fatigue 1999;21(Supplement 1):S199–209.
[47] Totten GE. Steel heat treatment: metallurgy and technologies. 2nd ed. Boca Raton, FL: Taylor & Francis; 2007.
[48] Fang Z. Wear resistance of powder metallurgy alloys. ASM International; 1998.
[49] Low-Alloy Carbon Steels. Metallic materials. CRC Press; 2003.
[50] Stellite 6 Alloy (Technical Data). <www.stellite.com>.
[51] Birol Y. Thermal fatigue testing of Stellite 6-coated hot work tool steel. Mater Sci Eng, A 2010;527:6091–7.